



**HAL**  
open science

# A highly efficient user-defined finite element for load distribution analysis of large-scale bolted composite structures

P.J. Gray, C.T. Mccarthy

► **To cite this version:**

P.J. Gray, C.T. Mccarthy. A highly efficient user-defined finite element for load distribution analysis of large-scale bolted composite structures. Composites Science and Technology, 2011, 10.1016/j.compscitech.2011.06.011 . hal-00786585

**HAL Id: hal-00786585**

**<https://hal.science/hal-00786585>**

Submitted on 9 Feb 2013

**HAL** is a multi-disciplinary open access archive for the deposit and dissemination of scientific research documents, whether they are published or not. The documents may come from teaching and research institutions in France or abroad, or from public or private research centers.

L'archive ouverte pluridisciplinaire **HAL**, est destinée au dépôt et à la diffusion de documents scientifiques de niveau recherche, publiés ou non, émanant des établissements d'enseignement et de recherche français ou étrangers, des laboratoires publics ou privés.

## Accepted Manuscript

A highly efficient user-defined finite element for load distribution analysis of large-scale bolted composite structures

P.J. Gray, C.T. McCarthy

PII: S0266-3538(11)00217-X  
DOI: [10.1016/j.compscitech.2011.06.011](https://doi.org/10.1016/j.compscitech.2011.06.011)  
Reference: CSTE 5011

To appear in: *Composites Science and Technology*

Received Date: 6 April 2011  
Revised Date: 16 June 2011  
Accepted Date: 19 June 2011

Please cite this article as: Gray, P.J., McCarthy, C.T., A highly efficient user-defined finite element for load distribution analysis of large-scale bolted composite structures, *Composites Science and Technology* (2011), doi: [10.1016/j.compscitech.2011.06.011](https://doi.org/10.1016/j.compscitech.2011.06.011)

This is a PDF file of an unedited manuscript that has been accepted for publication. As a service to our customers we are providing this early version of the manuscript. The manuscript will undergo copyediting, typesetting, and review of the resulting proof before it is published in its final form. Please note that during the production process errors may be discovered which could affect the content, and all legal disclaimers that apply to the journal pertain.



**A highly efficient user-defined finite element for load distribution analysis of large-scale bolted composite structures**

P.J. Gray, C.T. McCarthy<sup>1</sup>

*Materials and Surface Science Institute, Department of Mechanical and Aeronautical Engineering, University of Limerick, Ireland*

**Abstract**

This paper presents the development of a highly efficient user-defined finite element for modelling the bolt-load distribution in large-scale composite structures. The method is a combined analytical/numerical approach and is capable of representing the full non-linear load-displacement behaviour of bolted composite joints both up to, and including, joint failure. In the elastic range, the method is generic and is a numerical extension of a closed-form method capable of modelling the load distribution in single-column joints. A semi-empirical approach is used to model failure initiation and energy absorption in the joint and this has been successfully applied in models of single-bolt, single-lap joints. In terms of large-scale applications, the method is validated against an experimental study of complex load distributions in multi-row, multi-column joints. The method is robust, accurate and highly efficient, thus demonstrating its potential as a time/cost saving design tool for the aerospace industry and indeed other industries utilising bolted composite structures.

---

<sup>1</sup> Corresponding author. Tel.: +353-61-234334; fax: +353-61-202944. *Email address:* conor.mccarthy@ul.ie (C.T. McCarthy)

**Keywords:** A. Polymer-matrix composites (PMCs), B. Non-linear behaviour, C. Finite element analysis (FEA), Bolted joints

ACCEPTED MANUSCRIPT

## 1 Introduction

The efficiency of bolted joints is an essential consideration in the design of lightweight composite aircraft structures. Compared to their metal counterparts, carbon-fibre/epoxy joints experience a minimal amount of plastic stress relief around the hole and often fail catastrophically upon excessive loading. Many primary and secondary structures contain hundreds or potentially thousands of bolts. These structures often experience an uneven load distribution, thus compounding the complexity of the design problem. As a result, the overall approach to design tends to be over-conservative, resulting in the need for improved design methods where the emphasis is on reduced time and cost. This issue will be addressed in this paper, where a simplified numerical design tool has been developed for large-scale structural assemblies. The method will also be generic, i.e. it will have minimal reliance on experimental/numerical methods of calibration, thus making extensive design studies on bolted composite structures possible.

Joint design practices have been proposed in the past ranging from experimental testing [1-3], detailed three-dimensional finite element (3-D FE) analysis [4-10], analytical methods [11-15], boundary element formulations [16], boundary collocation methods [17] and semi-empirical approaches [18, 19]. Simplified FE approaches have been used to represent bolts and laminates [20-22]. For example, Ekh and Schön [20] used linear beam elements to model both the bolts and the laminates, while connector elements were used to capture bolt-clearance and bolt torque effects. The method was highly efficient but was limited to the modelling of single-column joints. Both Friberg [23, 24] and Gray and McCarthy [25] used beam elements with simplified contact models to model the bolt, while shell elements were used to represent the laminates. Both approaches required areas of high mesh refinement around the bolt-hole. In order to incorporate non-linear material behaviour, both models would suffer locally (i.e. close to the bolt-hole) from reduced increment sizes and excessive

equilibrium iterations in implicit versions of FE codes. In the authors' opinion, the problem of mesh dependency may be resolved by incorporating user-defined joint behaviour in global FE meshes. This involves removing local details from the mesh, such as bolts, washers, holes and contact models and replacing them with non-linear 'beam-type' elements with three-dimensional capability. This philosophy is only briefly addressed in the literature by McCarthy *et al.* [26], Gunnion *et al.* [27] and Pearce *et al.* [28]. In [27], rivets were represented by mesh-independent Point Link 'PLINK' elements in the PAM/CRASH FE code and simplified rivet failure laws were introduced for both in-plane shear (bearing) and out-of-plane tension (pull-through) loading on the bolt. Experimental tests were used to define the elastic stiffness and strength of the joint. This method of representing the fastener performed very well when the overall load-displacement behaviour of the model was compared to an experimental result. However, the load distribution has yet to be captured using this method, which is an important form of validation for global analysis tools. In addition, the method has yet to be extended to model non-linear elastic behaviour due to bolt-hole clearance and friction effects in the joint. And finally, the method was not generic, i.e. it relied entirely on experimental methods of calibration.

In this paper, a mesh-independent approach will be developed and validated, where a single 'user-defined finite element' will be used to represent the mechanical behaviour of the joint. The method will be generic in the elastic range, while a semi-empirical approach will be used to model non-linear material behaviour in the joint. The method has been implemented in the implicit solver of the commercially available FE code ABAQUS. The main aim of this paper is to predict the load distribution (i.e. bolt-hole contact loads and contact angles) in multi-row, multi-column joints to a good degree of accuracy, whilst maintaining a high level of computational efficiency.

## 2 Problem Description

### 2.1 Joint geometries and materials

The single-bolt, single-lap joint, shown in Fig.1(a), was used for the initial development of the user-defined finite element as extensive experimental and numerical results for this joint configuration were available from the literature [1, 4-6]. Following this study, the capability of the method to model complex load distributions will be assessed through a global FE analysis of a twenty-bolt joint (see Fig.1(b)) in both single-lap and double-lap joint configurations. The presence of a hole at the centre of the structure gives rise to a more complex load distribution i.e. increased presence of bolt-load components in both in-plane (i.e. X and Y) directions. Both joint configurations in Fig.1(a) and Fig.1(b) were used as benchmark studies in the EU Framework 5 project BOJCAS (Bolted Joints in Composite Aircraft Structures) [29]. The joints were fabricated using a carbon fibre/epoxy composite material manufactured by Hexcel composites, with designation HTA/6376. In the single-bolt, single-lap joint, both laminates had a quasi-isotropic lay-up with stacking sequence  $[45/0/-45/90]_{5s}$ . Each ply had a thickness of 0.13 mm, yielding a total laminate thickness of 5.2 mm. In the twenty-bolt case, the 3.12 mm and 6.24 mm thickness laminates had stacking sequences of  $[\pm 45/0/90]_{3s}$  and  $[\pm 45/0/90]_{6s}$ , respectively. Unidirectional lamina material properties are listed in Table 1. The variables  $E_{ii}$ ,  $G_{ij}$  and  $\nu_{ij}$  refer to the modulus, shear modulus and Poisson's ratio in the principle material directions  $i, j$  ( $i, j = 1, 2, 3$ ), respectively. In the user-defined finite element, the material was modelled using homogeneous material properties, which were obtained by McCarthy *et al.* [4] and are also listed in Table 1. The variables  $E_{nm}$ ,  $G_{nm}$  and  $\nu_{nm}$  refer to the modulus, shear modulus and Poisson's ratio in the global laminate directions  $n, m$  ( $n, m = x, y, z$ ), respectively. The 6 mm and 8 mm diameter bolts were made from aerospace grade Titanium alloy and the material properties (where  $E$  and  $\nu$ , refer to the Young's Modulus and Poisson's ratio, respectively) are again listed in Table 1.

## 2.2 Joint behaviour to be replicated by the user-defined finite element

The mechanical behaviour of the element is governed by the joint's load-displacement response and typical characteristics are illustrated in Fig.2(a). This curve is taken from an actual single-bolt, single-lap joint experiment carried out by McCarthy *et al.* [1]. In Fig.2(a), the area designated 'Elastic Region' represents the elastic behaviour of the joint. The initial quasi-linear region, dominated mainly by the shear stiffness of the laminate ( $K_{SHEAR}$ ), is due to static friction forces at the shear plane of the joint. With increased joint load, these static friction forces are overcome and the laminates begin to slip relative to each other. During this phase of loading, the large bolt-hole clearance ( $c$ ) is gradually taken up until the bolt shank begins to contact the hole. When significant contact is established, the bolt starts to transmit load and the bolt stiffness ( $K_{BOLT}$ ) is taken up. A more detailed description of bolt-hole clearance and friction effects is provided in [15].

As shown in Fig.2(a), the elastic displacement of the joint is denoted by  $u_{ELASTIC}$  and this quantity may be determined using a closed form approach that was developed by the authors in a previous publication [15]. To model failure initiation and energy absorption, designated as the 'Damage Region' in Fig.2(a), a semi-empirical approach is proposed. The point at which damage is said to initiate is the first significant failure load,  $P_{SF}$ , i.e. the point at which an abrupt change in joint stiffness occurs. For a given control case, either an experiment or a detailed numerical analysis can be used to plot the evolution of bearing stresses across the damage region, which can thus be used to equate failure loads (from Point A to Point B in Fig.2(a)) across a variety of joint thicknesses and hole diameters. The bearing stresses from the control case (and hence the joint strength and damage evolution stresses) may be plotted using the standard formula for bearing stress [1]:

$$\sigma_b = \frac{P_{control}}{D_{control} t_{control}} \quad (1)$$

where  $P_{control}$  is the load,  $t_{control}$  is the laminate thickness and  $D_{control}$  is the bolt diameter of the control case. For any joint of the same material and baseline stacking sequence (for example  $[45/0/-45/90]_i$  where  $i$  can be any positive integer), loads in the damage region may be determined by:

$$P = \sigma_b t D + P_{FRIC} \quad (2)$$

The first term of Eq.2 is the expression for bearing load (where  $\sigma_b$  is found using the control case), while the second term accounts for an offset in failure load due to friction forces in the joint ( $P_{FRIC}$ ). The value for  $P_{FRIC}$  can be predicted analytically [15]. The displacements to failure ( $u_{DAMAGE}$ ) may be solved using cubic spline interpolation [30] of failure loads from Point A to B. In this method, the damage region is split into  $m$  evenly spaced sub-intervals between  $u_{SF}$  and  $u_{FINAL}$  (i.e. the displacement at catastrophic failure) as shown in Fig.2(b). For convenience, the curve was broken up into five distinct regions ( $m = 5$ ). The joint stiffness at the first and last intervals ( $K_{JOINT_{(0)}}^{SF}$  and  $K_{JOINT_{(5)}}^F$ , respectively) are already known. The stiffness in the remaining intervals ( $K_{JOINT_{(N)}}$ , for  $N = 1, \dots, m - 1$ ) can be found by solving a system of linear spline equations of the type:

$$K_{JOINT_{(N-1)}} + 4K_{JOINT_{(N)}} + K_{JOINT_{(N+1)}} = \frac{3}{h}(P_{(N+1)} - P_{(N-1)}) \quad (3)$$

$$N = 1, \dots, m - 1$$

where  $h$  is the size of the displacement interval and  $P_{(N)}$  is the load at the  $N^{\text{th}}$  chosen point.

On every interval,  $P_{(N)} \leq P \leq P_{(N+1)}$ , the failure loads,  $P_{DAMAGE}^{(i)}$  (where  $i$  is the current load increment), are solved using a cubic polynomial of the form:

$$P_{DAMAGE}^{(i)} = a_{N0} + a_{N1}(u - u_{(N)}) + a_{N2}(u - u_{(N)})^2 + a_{N3}(u - u_{(N)})^3 \quad (4)$$

$$N = 1, \dots, m - 1$$

The coefficients  $a_{N0}$ ,  $a_{N1}$ ,  $a_{N2}$  and  $a_{N3}$  can be found using the Taylor series [30]:

$$\begin{aligned}
a_{N0} &= f_N(u_{-(N)}) = P_{-(N)} \\
a_{N1} &= f_N'(u_{-(N)}) = K_{-(N)} \\
a_{N2} &= \frac{1}{2} f_N''(u_{-(N)}) = \frac{3}{h^2} (P_{-(N+1)} - P_{-(N-1)}) - \frac{1}{h} (K_{-(N+1)} + 2K_{-(N)}) \\
a_{N3} &= \frac{1}{6} f_N'''(u_{-(N)}) = \frac{2}{h^3} (P_{-(N+1)} - P_{-(N-1)}) + \frac{1}{h^2} (K_{-(N+1)} + K_{-(N)})
\end{aligned} \tag{5}$$

The resulting cubic spline from the control case is illustrated by the dashed line in Fig.2(b).

The total joint displacement ( $u$ ) in load increment,  $i$ , is found using the summation of

$u_{ELASTIC}$ , which is found using the analytical model from [15], and  $u_{DAMAGE}^{(i)}$ .

### 2.3 Capabilities of the model

When considering failure initiation and energy absorption, the model is not fully generic. However, the model is highly efficient and is applicable to most joint design variables. In design cases where changes in baseline stacking sequence and fastener type are necessary, experiments or 3-D FE models must be used to calibrate failure initiation and energy absorption. Apart from these two variables, the model can account for changes in joint thickness, hole diameter, bolt-hole clearance and bolt torque. Laminate width and end-distance can also be captured, provided the joint is designed to fail in bearing. In the model, it is assumed that the laminate thickness, hole diameter and bolt-hole clearance have a negligible effect on the bearing strength of the joint. Kelly and Hallström [31] found that laminate thickness did not have a significant effect on the bearing strength of torqued (5 Nm) laminates, but a slight degree of variation existed when varying clearance cases were examined. McCarthy *et al.* [1] found that the presence of bolt-hole clearance only marginally affects the bearing strength of the joint and so, the assumptions made herein seemed reasonable.

### 3 Model Development

#### 3.1 Element behaviour

The concept of the user-defined finite element is illustrated in Fig.3(a). The overall load-displacement behaviour of the control volume (i.e. the material illustrated in Fig.1(a) and Fig.3(a)) is formulated analytically [15] and is governed by:

1. Shear loading in the X-direction
2. Shear loading in the Y-direction
3. Out-of-plane tension in the Z-direction

The control volume consists of the bolt, head, nut, hole, washers and joint foundation (composite material in the vicinity of the bolt-hole). In single-lap joints, this detailed region is replaced by a user-defined finite element, as shown in Fig.3(a), where the degrees of freedom (D1-D10) are employed to model the full three-dimensional behaviour of the control volume. On Node 1, degrees of freedom D1 and D2 represent translation of the joint in the X and Y directions, respectively, while D3 represents loading in the Z-direction. D4 and D5 represent rotations that are induced by secondary bending in the joint. The same reasoning is used for degrees of freedom D6 through D10 on Node 2. The user-defined element capability in ABAQUS was chosen due to its potential for efficient solution and its flexibility. For example, an extra node with two degrees of freedom can be placed along the length of the element to model double-lap joints, as shown in Fig.3(b).

The behaviour of the element is coded in the user-defined finite element subroutine UEL. In each increment and iteration, ABAQUS/Implicit provides values of nodal variables such as coordinates, displacements, incremental displacements, velocities and accelerations. The element's main contribution to the model is to provide prescribed nodal forces/moments for given displacements. In UEL, the relative displacement between Nodes 1 and 2 (for the single-lap case in Fig.3(a)) is recorded and a nodal force is interpolated from the element's

load-displacement curve. These nodal forces serve as internal reaction forces and this concept is illustrated in Fig.4. The typical loading regime of a single-bolt, single-lap joint is illustrated in Fig.4(a) where the external load contribution in a 3-D FE model is shown together with a simplified global model. The variables  $P_X$ ,  $M_Y$ , and  $P_Z$  represent the applied load in the global X-direction, the bending moment due to secondary bending and the reaction force due to bending at the gripped end of the laminates, respectively. The moment term ( $M_Y$ ) is simply equal to  $P_X$  multiplied by the joint eccentricity ( $e$ ) and is used to replicate the ‘tipping’ action of the bolt under an eccentric load path. The  $I_{MY}$  term represents the resulting reaction moment at the gripped end of the specimen. The internal reaction forces in the user-defined element (to enforce equilibrium in the joint) are illustrated in Fig.4(b), where  $I_{PX}$  represents the internal reaction force due to  $P_X$  and  $I_{PZ}$  represents the internal reaction force due to fastener pull-through.  $M_Y$  also serves as a coupling mechanism between shear loads (in this case  $I_{PX}$ ) and out-of-plane tension loads ( $I_{PZ}$ ), i.e. secondary bending induces tension in the bolt. In its current format, a detailed 3-D FE model has been used to characterise the load-displacement behaviour of the joint in the Z-direction. However, a highly efficient, spring-based formulation is currently under development.

The loading regime of a double-lap case is shown in Fig.4(c). In this case, half of the applied joint load ( $P_X / 2$ ) is experienced by the upper and lower splice plates. It is also assumed that a small bending moment ( $M_Y / 2$ ) is generated due to bending of the fastener. However, this contribution is minimal in comparison to the single-lap case and does not produce significant bolt tension loads and so,  $P_Z$  has been omitted here. To enforce equilibrium in the double-lap system, the internal forces induced by the user-defined element are illustrated in Fig.4(d).

### 3.2 Convergence control

As illustrated in Fig.2(a), the load-displacement behaviour of the joint is non-linear. ABAQUS/Implicit solves non-linear problems using the Newton-Raphson method [32]. In any non-linear analysis, multiple equilibrium iterations are often necessary to achieve convergence. The efficiency and stability of the user-defined element can be significantly improved with an accurate definition of the tangent stiffness ( $K_N$ ) in each displacement increment. Since  $P_N$  (and hence  $I_N$ ) are already known for a given displacement (from the joint's load-displacement curve), an accurate definition of  $K_N$  is possible. The load from the previous increment ( $N - 1$ ) can be stored as a solution dependant state variable (designated SDV in ABAQUS [32]) and a reasonable estimate of the tangent stiffness is found from:

$$K_N = \frac{I_N - I_{N-1}}{u_N - u_{N-1}} = \frac{\Delta I}{\Delta u} \quad (6)$$

This method of defining  $K_N$  is accurate (regardless of increment size) and was found to improve convergence considerably, thus resulting in a much more efficient solution.

Eq.6 represents the tangent stiffness in one dimension, but since the problems in Fig.3 are three-dimensional,  $K_N$  must be written as:

$$K_{iakb} \Delta u_k^b = \Delta I_i^a \quad (7)$$

where  $i$  and  $k$  represent degrees of freedom, and  $a$  and  $b$  represent the node number. In the single-lap user-defined element in Fig.3(a), there are two nodes with five degrees of freedom per node. Therefore  $K_{iakb}$  is a 10 X 10 tangent stiffness matrix in the single-lap case and specific terms of  $K_{iakb}$  are calculated for the current increment. For example, if a positive displacement is applied to Node 2 in the X-direction only ( $u_6^2$ ), the tangent stiffness term  $K_{6262}$  may be written as:

$$K_{6262} = \left. \frac{\Delta I}{\Delta u} \right|_{X-Dir} \quad (8)$$

where the  $\Delta I$  and the  $\Delta u$  terms are found using the method outlined in Fig.5 and applying it to the load-displacement curve in the X-direction. Note that the  $\Delta u$  term is passed in for information by UEL and is equal to the relative incremental displacement between Nodes 1 and 2.  $K_{6262}$  effectively represents the tangent stiffness of the joint due to shear loading in the X-direction for the current increment  $N$ . Similarly, the terms  $K_{1162}$ ,  $K_{1111}$  and  $K_{6211}$  are written as:

$$K_{1162} = K_{1111} = K_{6211} = \frac{\Delta I}{\Delta u} \Big|_{X-Dir} \quad (9)$$

All other terms in the stiffness matrix would be set to zero and  $K_{iakb}$  would take the following form:

$$\begin{bmatrix} K_{1111} & 0 & 0 & 0 & 0 & -K_{1162} & 0 & 0 & 0 & 0 \\ 0 & 0 & 0 & 0 & 0 & 0 & 0 & 0 & 0 & 0 \\ 0 & 0 & 0 & 0 & 0 & 0 & 0 & 0 & 0 & 0 \\ 0 & 0 & 0 & 0 & 0 & 0 & 0 & 0 & 0 & 0 \\ 0 & 0 & 0 & 0 & 0 & 0 & 0 & 0 & 0 & 0 \\ -K_{6211} & 0 & 0 & 0 & 0 & K_{6262} & 0 & 0 & 0 & 0 \\ 0 & 0 & 0 & 0 & 0 & 0 & 0 & 0 & 0 & 0 \\ 0 & 0 & 0 & 0 & 0 & 0 & 0 & 0 & 0 & 0 \\ 0 & 0 & 0 & 0 & 0 & 0 & 0 & 0 & 0 & 0 \\ 0 & 0 & 0 & 0 & 0 & 0 & 0 & 0 & 0 & 0 \end{bmatrix} \begin{bmatrix} \Delta u_1^1 \\ 0 \\ 0 \\ 0 \\ 0 \\ \Delta u_6^2 \\ 0 \\ 0 \\ 0 \\ 0 \end{bmatrix} = \begin{bmatrix} \Delta I_1^1 \\ 0 \\ 0 \\ 0 \\ 0 \\ \Delta I_6^2 \\ 0 \\ 0 \\ 0 \\ 0 \end{bmatrix} \quad (10)$$

In order to capture multi-axial loads applied to the joint, a similar procedure is followed for loads in the global Y and Z directions and other terms of  $K_{iakb}$  are populated.

### 3.3 Boundary conditions and loading

A plot of the global mesh for the single-bolt, single-lap joint is illustrated in Fig.3(c), in which details such as boundary conditions and coupling constraints are included. To represent the gripped end of the joint, both translational degrees of freedom ( $u_x$ ,  $u_y$  and  $u_z$ ) and rotational degrees of freedom ( $\theta_x$ ,  $\theta_y$ ,  $\theta_z$ ) at the leftmost end of the specimen are constrained. At the rightmost end, a displacement is prescribed in the X-direction to induce load into the joint, while the remaining degrees of freedom ( $u_y$ ,  $u_z$ ,  $\theta_x$ ,  $\theta_y$ ,  $\theta_z$ ) are

constrained. The forces and moments are transmitted from the user-defined element to the global mesh using distributed coupling constraints as shown in Fig.3(c). The size of the coupling region is set equal to the size of the joint control volume shown in Fig.3(a) or Fig.3(b). This coupling technique also mitigates mesh sensitivity effects in the model. To complete the model, a surface-to-surface type contact definition was used between the upper and lower plates. The friction coefficient was set to zero in this contact definition, as friction in the joint region is accounted for in the closed-form model from [15]. Given the relative coarseness of the mesh, it was found that this contact model did not significantly affect computational efficiency. The elements that were used in the global model (in Fig.3(c)) were layered shell elements with reduced integration (designated S4R in ABAQUS [32]). In order to ensure that the full mechanical behaviour of the joint was captured, a simple continuum damage model developed by Lapczyk and Hurtado [33] was used in the global mesh. Material strength values for the global mesh are listed in Table 1 (where  $S_{ii}^T$  and  $S_{ii}^C$  refer to strength in the principle material directions  $i$  ( $i = 1, 2$ ) for tensile ( $T$ ) and compressive loading ( $C$ ), respectively). The variables  $S_{ij}$  refer to shear strengths in the principle material directions  $i, j$  ( $i, j = 1, 2$ ). However, it was found that, in all cases, failure of the joint was dictated entirely by the user-defined finite element.

#### 4 Model Validation

The user-defined finite element has been validated against experimental results from the single-bolt, single-lap joint in Fig.1(a) and the effect of varying bolt-hole clearance and bolt torque from [1] was examined. Both neat-fit (10  $\mu\text{m}$ ) and large (240  $\mu\text{m}$ ) bolt-hole clearances were considered and 7.2 MPa (finger-tight torque [6]) and 227 MPa (high torque [6]) pre-stresses were prescribed to the bolt. The load-displacement behaviour of all clearance and torque cases examined herein are illustrated in Fig.6(a) to Fig.6(d). The effects of bolt-hole clearance and bolt torque are captured quite well by the model. In

Fig.6(b), a delay in load take-up approximately equal to the bolt-hole clearance of 240  $\mu\text{m}$  has been captured by the model. Comparing Fig.6(d) to Fig.6(b), this delay in load take-up occurs at a higher load level due to friction effects early in the loading history. In Fig.6(d), a comparably higher bolt pre-stress of 227 MPa was used. As discussed in [15], high bolt pre-stresses induce *sticking* between the laminates earlier in the loading history, and in this case, the transition from *sticking* to *slipping* occurs at approximately 5kN joint load. The presence of this critical friction force ( $P_{FRIC}$ ) is less obvious when comparing the low 10  $\mu\text{m}$  clearance cases of Fig.6(a) and Fig.6(c). Good agreement was obtained between the global model and the experiments [1] in terms of joint strength and energy absorption. Comparing Fig.6(a) to Fig.6(c), the bearing strength of the joint is exceeded at approximately 21 kN in the finger-tight case, while in the highly torqued joint, it occurs at approximately 26 kN. This offset in joint strength is primarily due to the critical friction force,  $P_{FRIC}$ . The results in Fig.6 demonstrate that the user-defined finite element can be used to model *any* type of non-linear behaviour in joints, ranging from bolt-hole clearance and friction forces early in the loading history to joint failure and energy absorption in the latter phases of loading.

## 5 Load distribution study

The capability of the element to model complex load distributions in multi-row, multi-column joints was also investigated. An elastic analysis of the twenty-bolt benchmark in Fig.1(b) was conducted for this purpose. To validate the model, strain distribution results from experimental work carried out by an industrial partner in the BOJCAS project [24] has been used as a basis for comparison. It should be noted that due to large deformations in the problem, large-strain theory (designated NLGEOM in ABAQUS [32]) was used to solve the problem. In addition, 10  $\mu\text{m}$  bolt-hole clearances and 7.2 MPa bolt pre-stresses were applied to the user-defined element. A FE mesh of the single-lap global model is shown in Fig.7(a) together with a plot of the shear strain distribution in the +45° plies at the shear

plane of the joint. The presence of the hole and the user-defined elements results in a non-uniform distribution of shear strain in the structure. Comparing Fig.7(a) to Fig.7(b) it can be seen that the double-lap joint tends to undergo much less out-of-plane deformation than the single-lap case. In order to compare the strain distribution in the global FE mesh to experiments and other numerical results, a numbering convention for the strain gauges is shown in Fig.7(c). The fastener numbering system is illustrated in Fig.1(b) and Fig.9. In addition to fully assembled models, the change in strain response due to the omission of certain fasteners around the structure has also been investigated. The joint configurations analysed are presented in Table 2 and the results from this study are illustrated in Fig.8. The single-lap joints were loaded to 250 kN, while a compressive load of 200kN was applied to the double-lap joint (as shown in Fig.7(b)).

Remarkable agreement was achieved between the global model, the experiment and Friberg's Method [24] as shown in Fig.8. Given that bolt-holes are not modelled discretely by the user-defined element, the accuracy of the global model is surprising. The close proximity of the strain gauges to each bolt-hole would suggest that the user-defined element would suffer some form of inaccuracy. However, Fig.8 clearly illustrates that this problem does not exist. Looking more closely at the result from Joint A, a peak in strain is visible at Bolt 13 in Gauges 9 and 10, suggesting that a significant portion of the by-pass load (around the hole at the centre of the structure) occurs at this location. In Joint B, Bolt 13 was removed and again good agreement was obtained between the experiment and the two analysis methods. In Joint C, Bolts 19 and 20 were removed and this seems to result in a shift in the peak strain towards Gauges 5 and 6 at Bolt 19. In Joint D, good correlation was found between the global model and Friberg's method [24]. However, results from both numerical models were found to deviate significantly from experimental results. In

general, the removal of bolts seems to result in a shift in the strain distribution and in order to understand this behaviour, a load distribution analysis of the joints was carried out.

The results from the load distribution analysis are illustrated in Fig.9, where the percentages of the total joint load carried by each fastener in the structure are presented together with bolt-hole contact angles. Comparison with load distributions from experimental results was not possible as results from tests involving instrumented fasteners were not available. However, load distribution results from the fully validated numerical approach of Friberg [23,24] were available and have thus been used for the purposes of comparison in this paper. Regarding Joint A, excellent agreement between the global model and Friberg's Method [24] was obtained in terms of the load sharing capacity of each individual fastener. A degree of fluctuation in the percentage of load carried is seen between Bolts 6 and 10. It should be noted that the fasteners located quite close to the hole at the centre of the structure (such as Bolts 7, 8, 10, 11, 13 and 14) experience relatively low bolt-loads. In terms of the bolt-load angles (which were computed from components of bolt-load acting in the X and Y directions at each fastener location), good agreement was also obtained between the global model and Friberg's model [24]. It can be clearly seen that bolts located away from the hole at the centre of the structure experience high contact angles, while bolts located on the X-axis of symmetry experience very low contact angles.

In Joint B, the presence of a missing fastener at location 13 results in a notable change in the load distribution. Fasteners located in the lower half of the structure take a higher portion of the overall joint load and experience slightly higher contact angles. This effect was captured quite well by both the global model and Friberg's Method. In Joint C, missing bolts at locations 19 and 20 result in a redistribution of load to Bolts 16, 17 and 18 and again good agreement was obtained between both methods of load distribution analysis.

This would suggest that the removal of bolts results in a localised effect, where bolts which are located close to open holes carry more load. The results from Joint D demonstrate that the user-defined element can also be successfully applied to large-scale double-lap joints.

## 6 Computational efficiency

Simplified global models of single-bolt, single-lap joints displayed excellent CPU times as shown in Table 3. Each analysis was run on a single processor in a dual-core, 3.5GB RAM personal computer (Intel® Core™ 2 CPU, 2.13GHz). For example, the CPU run-time for the 240 $\mu$ m clearance, 16 Nm joint was 43 seconds. Depending on the complexity of the damage model and solution scheme used, 3-D FE simulations of single-bolt joints can take hours or days to run. This is further hampered by time consuming friction models, which also require extensive iteration to achieve system equilibrium. It was also noted during analysis that the solution was highly stable, suggesting that the convergence control (tangent stiffness definition) imposed on the user-defined element during the non-linear solution scheme functioned very well. The twenty-bolt models also display excellent run-times, where global load distribution results were achieved with a high degree of accuracy and efficiency.

## 7 Concluding Remarks

In this paper, a highly efficient user-defined finite element for global load distribution analysis of bolted composite structures has been presented. The element is capable of representing any type of non-linear load-displacement behaviour of bolted composite joints ranging from bolt-hole clearance and friction effects to eventual joint failure. In the elastic range, the method is generic, where the elastic load-displacement response of the user-defined element is formulated using a closed-form analytical method developed in [15], while the onset of failure and damage evolution is modelled using a semi-empirical approach. The overall model is robust, accurate and highly efficient, where solution times

to large-scale problems can be achieved in minutes. The model captured strain distributions and complex load distributions in twenty-bolt joints to a good degree of accuracy. The redistribution of load due to missing fasteners was also captured well by the model and it was found that this redistribution is localised (i.e. fasteners located close to the open hole(s) become more highly loaded). Furthermore, the method is applicable to a variety of joint configurations and loading scenarios, thus demonstrating its capability as an industrial design tool. This approach could potentially be used for time and cost savings in the design of large-scale composite aircraft structures and could be used to maximise joint efficiency, thus demonstrating its immediate industrial significance.

### **Acknowledgements**

This work was funded by the Irish Research Council for Science, Engineering and Technology (IRCSET) and Airbus UK. The author would also like to acknowledge BOJCAS [29] for the permitted use of benchmark models and experimental results for the purposes of this paper. BOJCAS was an RTD project partially funded by the European Union under the European Commission GROWTH programme, Key Action: New Perspectives in Aeronautics, Contract No. G4RD-CT99-00036.

## References

- [1] McCarthy MA, Lawlor VP, Stanley WF and McCarthy CT. Bolt-hole clearance effects and strength criteria in single-bolt, single-lap, composite bolted joints. *Composites Science and Technology* 2002; 62(10-11): 1415-1431.
- [2] McCarthy MA, Lawlor VP and Stanley WF. An experimental study of bolt-hole clearance effects in single-lap, multi-bolt composite joints. *Journal of Composite Materials* 2005; 39(9): 799-825.
- [3] Lawlor VP, McCarthy MA and Stanley WF. An experimental study of bolt-hole clearance effects in double-lap, multi-bolt composite joints. *Composite Structures* 2005; 71(2): 176-190.
- [4] McCarthy MA, McCarthy CT, Lawlor VP and Stanley WF. Three-dimensional finite element analysis of single-bolt, single-lap composite bolted joints: Part I - model development and validation. *Composite Structures* 2005; 71(2): 140-158.
- [5] McCarthy CT and McCarthy MA. Three-dimensional finite element analysis of single-bolt, single-lap composite bolted joints: Part II - effects of bolt-hole clearance. *Composite Structures* 2005; 71(2): 159-175.
- [6] McCarthy CT, McCarthy MA, Stanley WF and Lawlor VP. Experiences with modelling friction in composite bolted joints. *Journal of Composite Materials* 2005; 39(21): 1881-1908.
- [7] Padhi GS, McCarthy MA and McCarthy CT. BOLJAT: A tool for designing composite bolted joints using three-dimensional finite element analysis. *Composites Part A - Applied Science and Manufacturing* 2002; 33(11): 1573-1584.
- [8] Camanho PP, Fink A, Obst A, and Pimenta S. Hybrid titanium-CFRP laminates for high-performance bolted joints. *Composites Part A - Applied Science and Manufacturing*. 2009; 40(12): 1826-1837.
- [9] Camanho PP and Matthews FL. A progressive damage model for mechanically fastened joints in composite laminates. *Journal of Composite Materials* 1999; 33(24): 2248-2280.
- [10] McCarthy CT, McCarthy MA and Lawlor VP. Progressive damage analysis of multi-bolt composite joints with variable bolt-hole clearances. *Composites Part B-Engineering* 2005; 36(4): 290-305.
- [11] Tate MB and Rosenfeld SJ. Preliminary investigation of the loads carried by individual bolts in bolted joints. NACA TN 1051, 1946.
- [12] Barrois W. Stresses and displacements due to load-transfer by fasteners in structural assemblies. *Engineering Fracture Mechanics* 1978; 10(1): 115-176.
- [13] Nelson WD, Bunin BL and Hart-Smith LJ. Critical joints in large composite aircraft structure. NASA CR-3710, 1983.
- [14] McCarthy MA, McCarthy CT and Padhi GS. A simple method for determining the effects of bolt-hole clearance on load distribution in single-column, multi-bolt composite joints. *Composite Structures* 2006; 73(1): 78-87.
- [15] McCarthy CT and Gray PJ. An analytical model for the prediction of load distribution in highly torqued multi-bolt composite joints. *Composite Structures* 2011; 92(2): 287-298.
- [16] Zhang JM. Design and analysis of mechanically fastened composite joints and repairs. *Engineering Analysis with Boundary Elements* 2001; 25(6): 431-441.
- [17] Madenci E, Shkarayev S, Sergeev B, Oplinger DW and Shyprykevich P. Analysis of composite laminates with multiple fasteners. *International Journal of Solids and Structures* 1998; 35(15): 1793-1811.

- [18] Barut A and Madenci E. Analysis of bolted-bonded composite single-lap joints under combined in-plane and transverse loading. *Composite Structures* 2009; 88(4): 579-594.
- [19] Huth H. Influence of fastener flexibility on the prediction of load transfer and fatigue life for multiple-row fasteners. *American Society for Testing and Materials*, Philadelphia; 1986; 927: 221-250.
- [20] Ekh J and Schön J. Finite element modeling and optimization of load transfer in multi-fastener joints using structural elements. *Composite Structures* 2008; 82(2): 245-256.
- [21] Eriksson I, Backlund J, and Moller P. Design of multiple-row bolted composite joints under general in-plane loading. *Composites Engineering*. 1995; 5(8): 1051-1068.
- [22] Ramkumar RL, Saether ES, and Appa K. Strength analysis of laminated and metallic plates bolted together by many fasteners. Air Force Wright Aeronautical Laboratories Technical Report. AFWAL-TR-86-3034. 1984.
- [23] Friberg M. Fastener load distribution and interlaminar stresses in composite laminates. Licentiate Thesis, Royal Institute of Technology: Stockholm, 2000.
- [24] Friberg M. Final description of global design methods developed. BOJCAS Tech. Report. Deliverable No: D2.3-4, 2002.
- [25] Gray PJ and McCarthy CT. A global bolted joint model for finite element analysis of load distributions in multi-bolt composite joints. *Composites Part B-Engineering*. 2010; 41(4): 317-325.
- [26] McCarthy MA, Xiao JR, McCarthy CT, Kamoulakos A, Ramos J, Gallard JP, and Melito V. Modelling bird impacts on an aircraft wing - Part 2: Modelling the impact with an SPH bird model. *International Journal of Crashworthiness*. 2005; 10(1): 51-59.
- [27] Gunnion AJ, Körber H, Elder DJ, and Thomson RS. Development of fastener models for impact simulation of composite structures. 25th Congress of the International Council of Aeronautical Sciences ICAS, Hamburg, Germany, 2006.
- [28] Pearce GM, Johnson AF, Thomson RS, and Kelly DW. Numerical investigation of dynamically loaded bolted joints in carbon fibre composite structures. *Applied Composite Materials*. 2010; 17(3): 329-346.
- [29] McCarthy MA. BOJCAS: Bolted Joints in Composite Aircraft Structures. *Air and Space Europe*. 2001; 3/4(3): 139-142.
- [30] McCarthy CT, O'Higgins RM, and Frizzell RM. A cubic spline implementation of non-linear shear behaviour in three-dimensional progressive damage models for composite laminates. *Composite Structures*. 2010; 92(1): 173-181.
- [31] Kelly G and Hallström S. Bearing strength of carbon fibre/epoxy laminates: effects of bolt-hole clearance. *Composites Part B-Engineering*. 2004; 35(4): 331-343.
- [32] ABAQUS Analysis User's Manual. Version 6.9. Dassault Systèmes 2010.
- [33] Lapczyk I and Hurtado JA. Progressive damage modelling in fibre-reinforced materials. *Composites Part A-Applied Science and Manufacturing*. 2007; 28: 2333-2341.

**Table 1 Material properties**

|   |                     |                     |                     |                     |                   |                   |            |            |            |
|---|---------------------|---------------------|---------------------|---------------------|-------------------|-------------------|------------|------------|------------|
| <b>Unidirectional properties for HTA/6376</b>                     | $E_{11}$<br>(GPa)   | $E_{22}$<br>(GPa)   | $E_{33}$<br>(GPa)   | $G_{12}$<br>(GPa)   | $G_{13}$<br>(GPa) | $G_{23}$<br>(GPa) | $\nu_{12}$ | $\nu_{13}$ | $\nu_{23}$ |
|   | 140                 | 10                  | 10                  | 5.2                 | 5.2               | 3.9               | 0.3        | 0.3        | 0.5        |
| <b>Homogenised laminate properties for quasi-isotropic lay-up</b> | $E_{xx}$<br>(GPa)   | $E_{yy}$<br>(GPa)   | $E_{zz}$<br>(GPa)   | $G_{xy}$<br>(GPa)   | $G_{xz}$<br>(GPa) | $G_{yz}$<br>(GPa) | $\nu_{xy}$ | $\nu_{xz}$ | $\nu_{yz}$ |
|   | 54.25*              | 54.25*              | 12.59               | 20.72*              | 4.55              | 4.55              | 0.309*     | 0.332      | 0.332      |
| <b>Material strength for HTA/6376</b>                             | $S_{11}^T$<br>(MPa) | $S_{11}^C$<br>(MPa) | $S_{22}^T$<br>(MPa) | $S_{22}^C$<br>(MPa) | $S_{12}$<br>(MPa) | $S_{23}$<br>(MPa) |            |            |            |
|   | 2170                | 1600                | 73                  | 250                 | 83                | 50                |            |            |            |
| <b>Titanium properties</b>  | $E$<br>(GPa)        | $\nu$               |                     |                     |                   |                   |            |            |            |
|   | 110                 | 0.29                |                     |                     |                   |                   |            |            |            |

\*Verified by classical laminate theory

**Table 2 Joint configurations**

| Joint | Joint Type | Description           | Loading     |
|-------|------------|-----------------------|-------------|
| A     | Single-lap | All bolts present     | Tension     |
| B     | Single-lap | Bolt 13 removed       | Tension     |
| C     | Single-lap | Bolts 19 & 20 removed | Tension     |
| D     | Double-lap | All bolts present     | Compression |

**Table 3 CPU run-times for 3D-FE models (dual-core, 3.5GB RAM CPU)**

| Model  | Joint Type        | Bolt-hole Clearance ( $\mu\text{m}$ ) | Bolt Torque (Nm) | Loaded to Failure? | CPU time (seconds) |
|--------|-------------------|---------------------------------------|------------------|--------------------|--------------------|
| Global | SBSL <sup>a</sup> | 10                                    | 0.5              | Yes                | 39                 |
| Global | SBSL <sup>a</sup> | 240                                   | 0.5              | Yes                | 32                 |
| Global | SBSL <sup>a</sup> | 10                                    | 16               | Yes                | 50                 |
| Global | SBSL <sup>a</sup> | 240                                   | 16               | Yes                | 43                 |
| Global | TBSL <sup>b</sup> | 10                                    | 0.5              | No                 | 254                |
| Global | TBSL <sup>b</sup> | 10                                    | 0.5              | No                 | 222                |
| Global | TBSL <sup>b</sup> | 10                                    | 0.5              | No                 | 310                |
| Global | TBDL <sup>c</sup> | 10                                    | 0.5              | No                 | 373                |

<sup>a</sup> SBSL- Single-bolt, single-lap<sup>b</sup> TBSL- Twenty-bolt, single-lap<sup>c</sup> TBDL- Twenty-bolt, double-lap

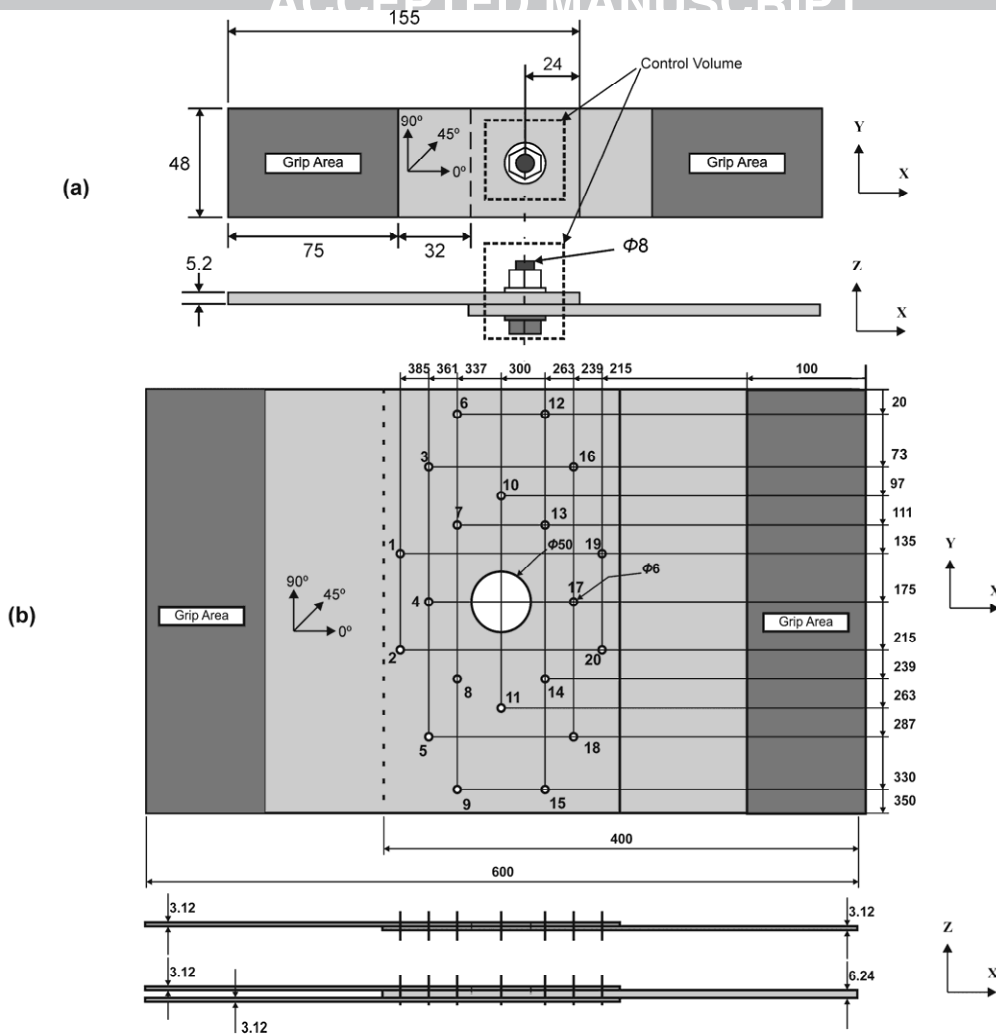


Fig. 1 Joint geometry (all dimensions in mm): (a) single-bolt, single-lap joint (redrawn from [1]); (b) twenty-bolt, single-lap and double-lap joints with bolt numbering system (redrawn from [24])

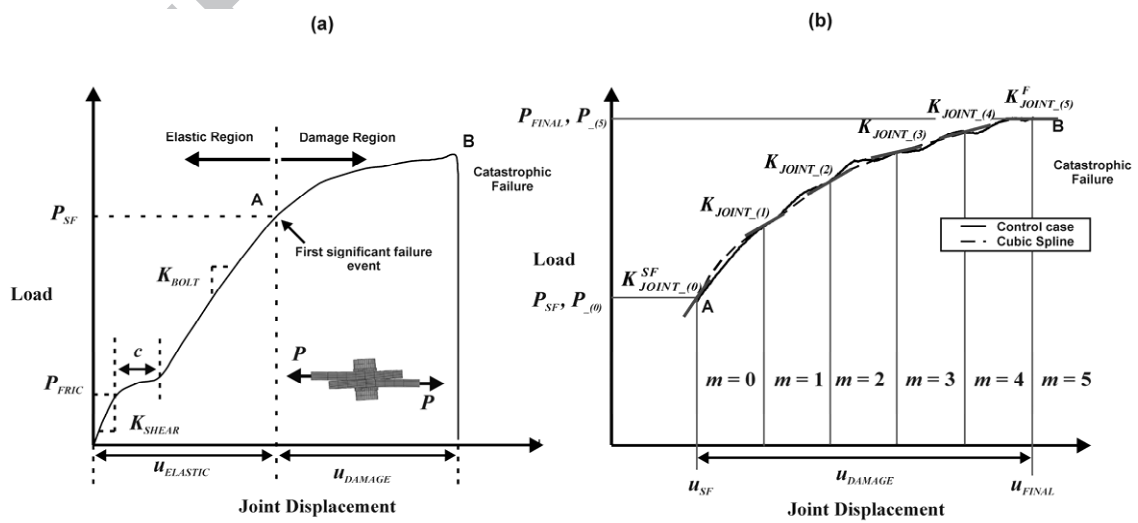


Fig. 2 Experimental load-displacement curve from a clearance-fit, highly torqued, single-bolt, single-lap joint: (a) total load-displacement behaviour (redrawn from [1]); (b) spline interpolation of failure loads

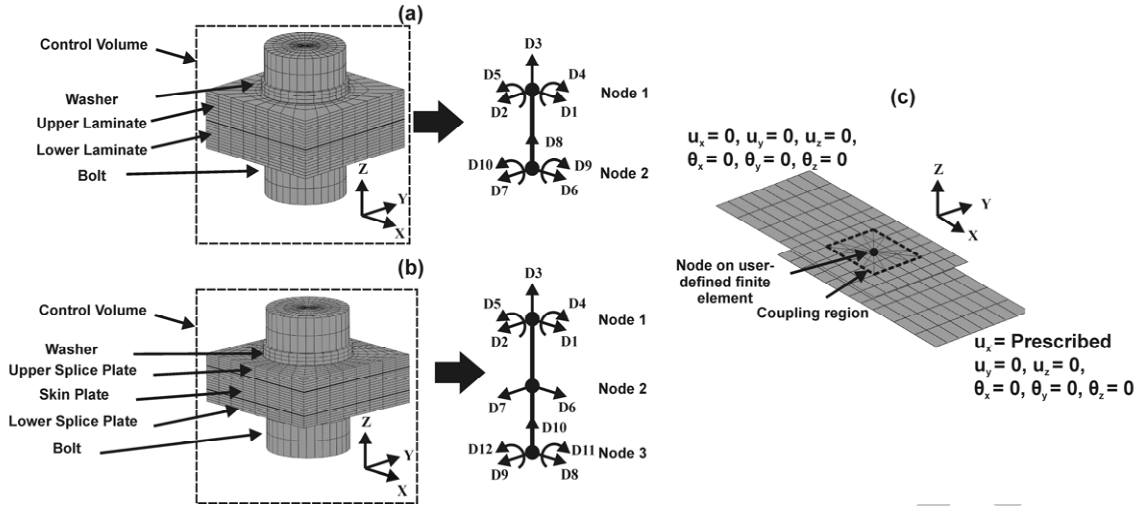


Fig. 3 Concept of the user-defined finite element: (a) single-lap configuration; (b) double-lap configuration; (c) finite element mesh and boundary conditions in a single-bolt, single-lap joint

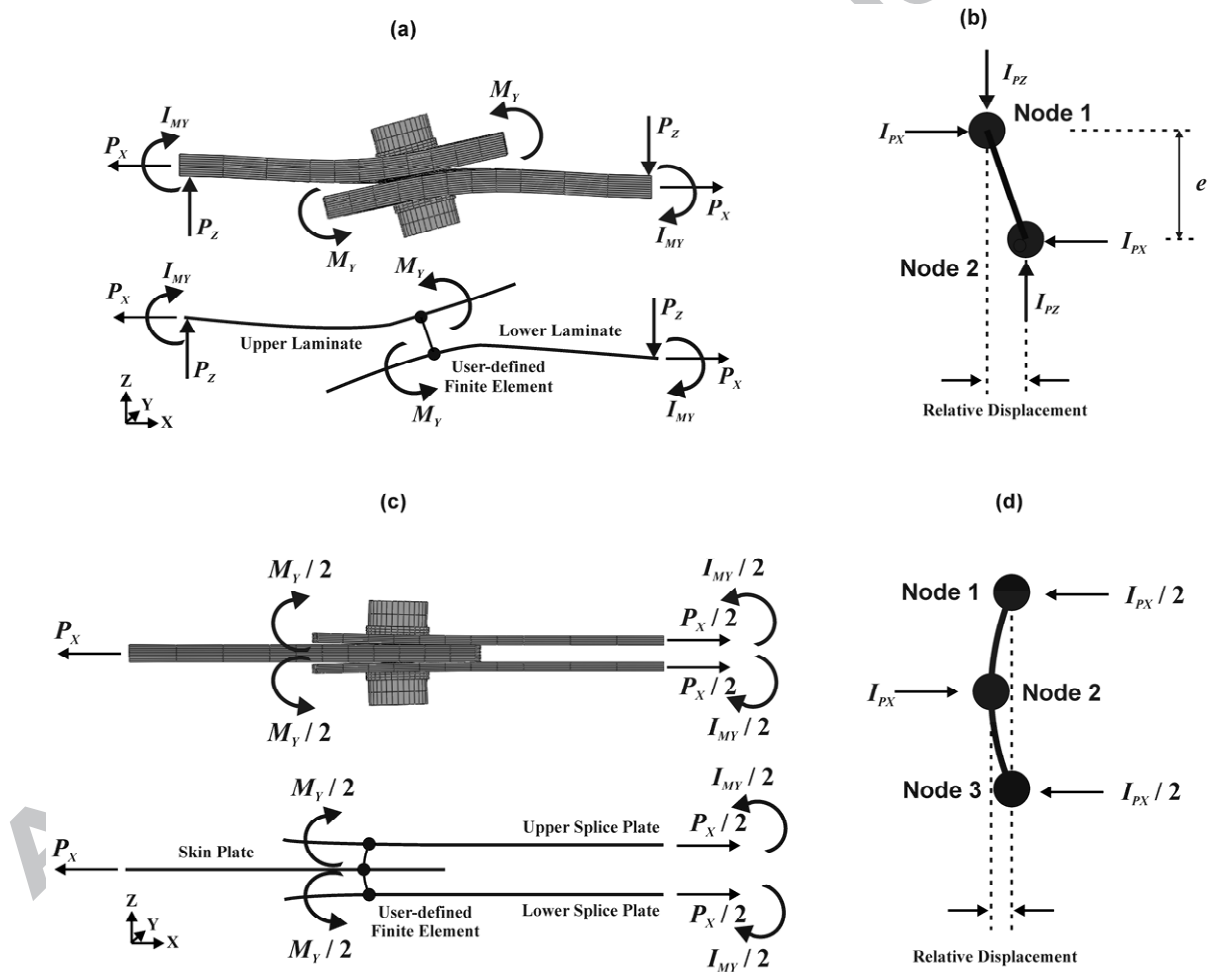


Fig. 4 Uni-axial loading and deformation of single-bolt joints: (a) forces and moments in a 3-D FE model and global model (single-lap); (b) internal reaction forces and moments in a single-lap user-defined finite element; (c) forces and moments in a 3-D FE model and global model (double-lap); (d) internal reaction forces and moments in a double-lap user-defined finite element

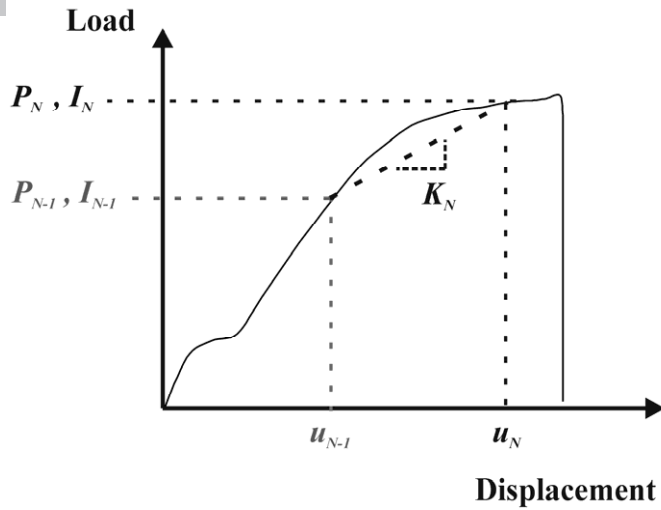


Fig. 5 Convergence control: tangent stiffness definition for the user-defined finite element

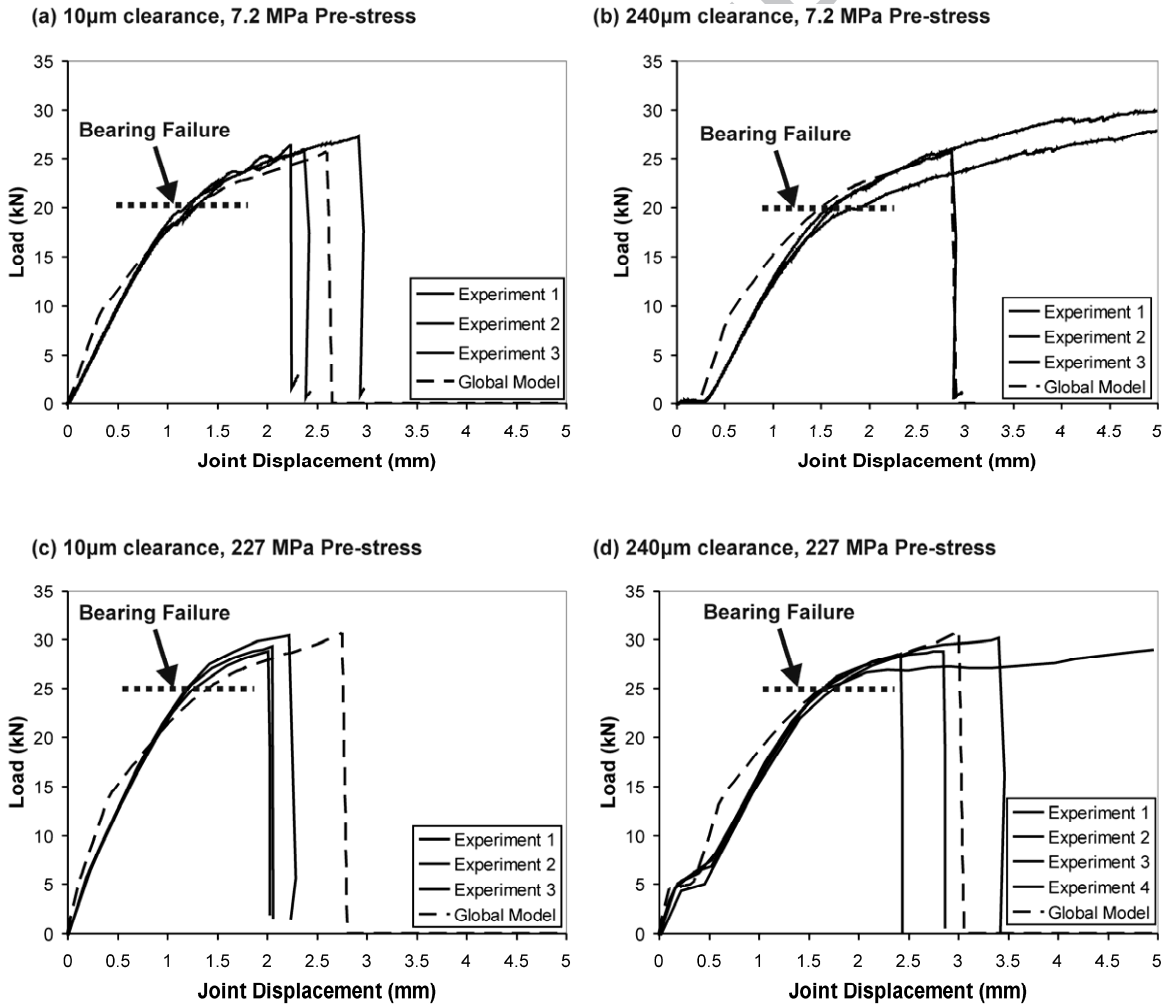


Fig. 6 Effect of varying bolt-hole clearance and torque on the elastic behaviour and damage development in single-bolt, single-lap joints (experiments [1] and global models)

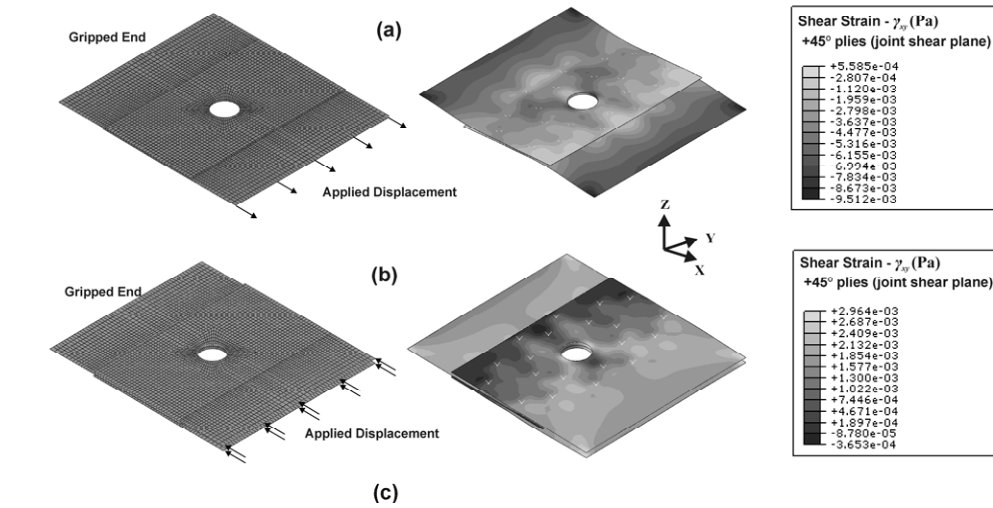


Fig. 7 Finite element mesh and deformation of twenty-bolt joints: (a) single-lap joint with shear strain distribution; (b) double-lap joint with shear strain distribution; (c) strain gauge numbering system (redrawn from [24])

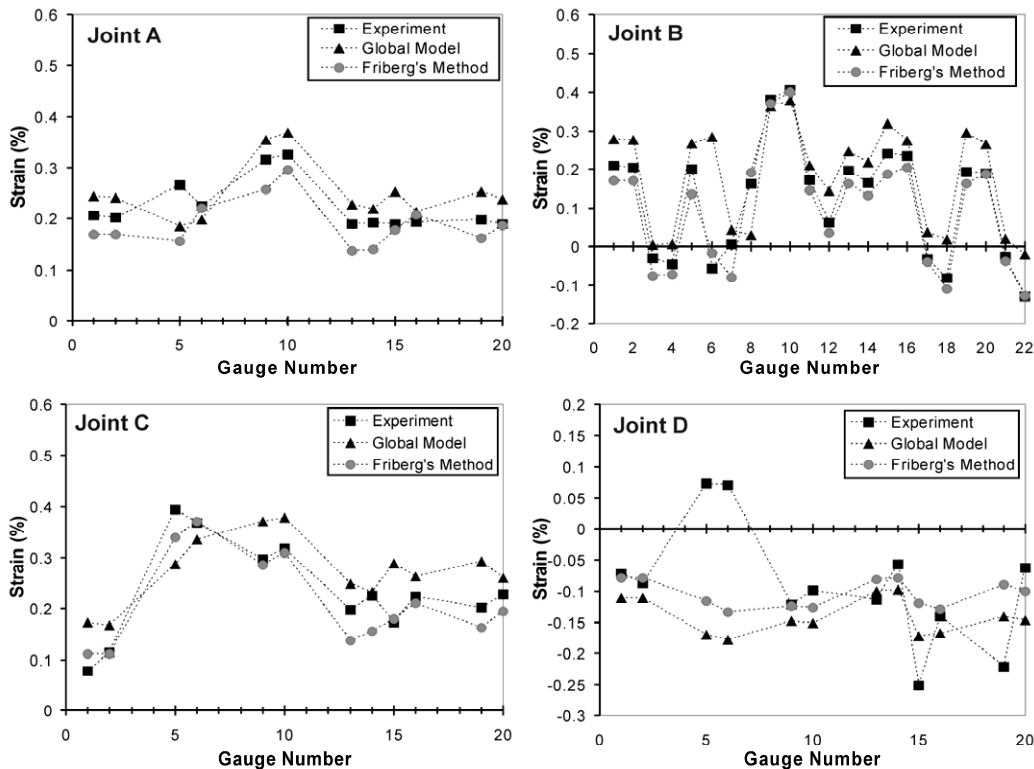


Fig. 8 Strain distribution in twenty-bolt joints (results from experiment and Friberg's Method redrawn from [24])

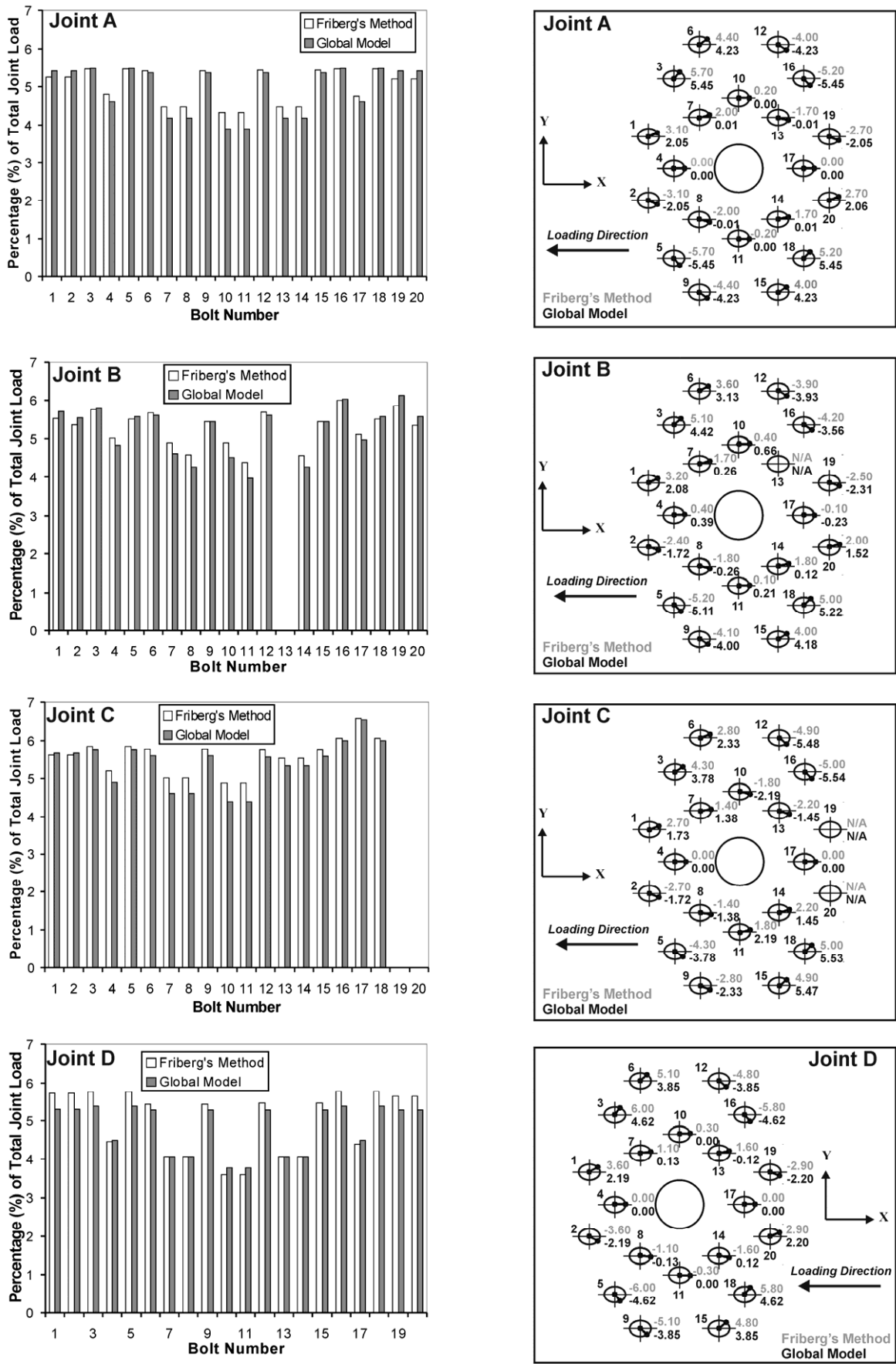
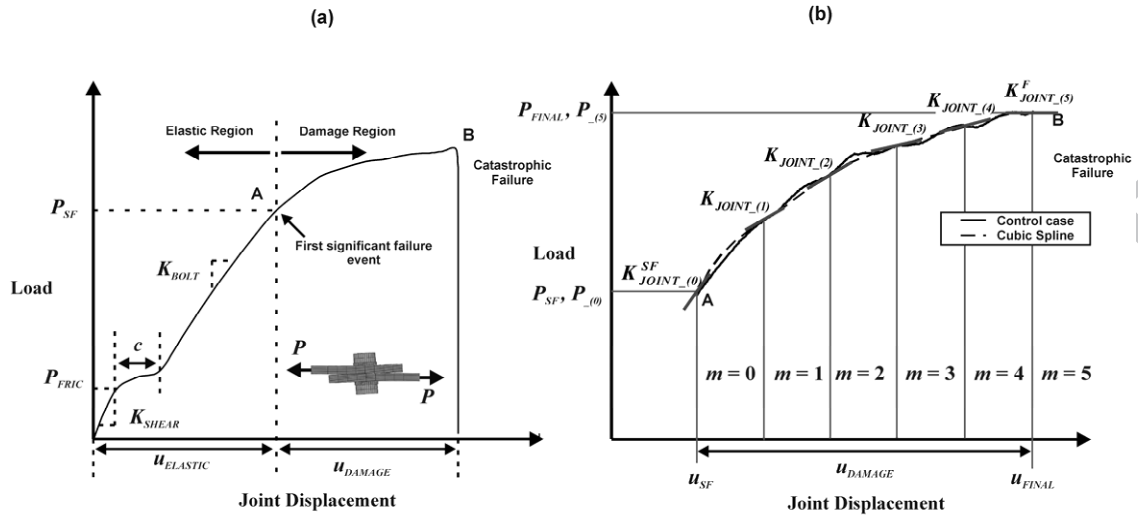


Fig. 9 Load distributions in twenty-bolt joints - percentage of load carried by each bolt and bolt-load angles (Friberg's Method redrawn from [24])

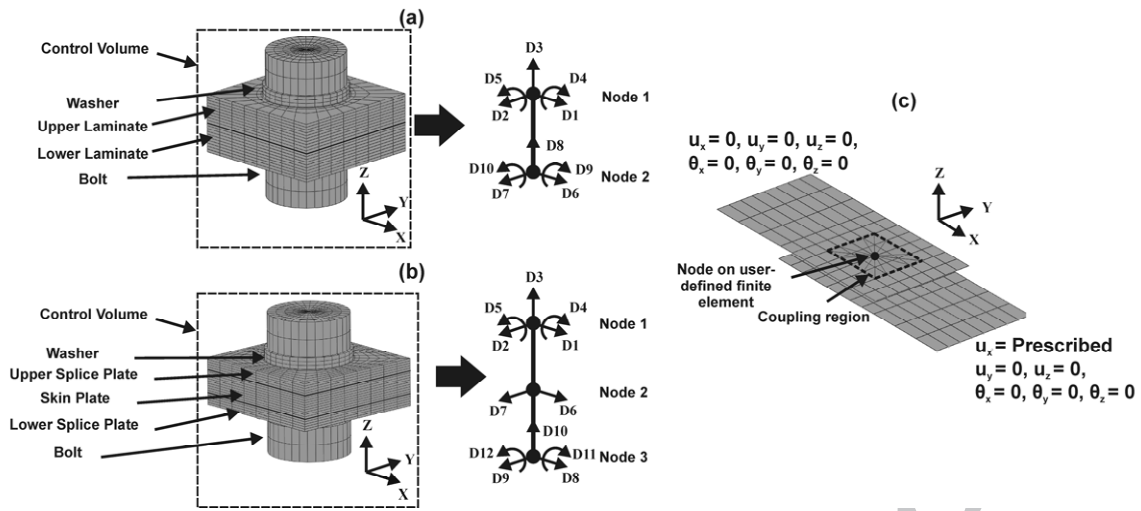
- A user-defined finite element for modelling bolted composites joints is presented
- The element represents non-linear load-displacement behaviour of single-bolt joints
- A combined analytical/numerical approach is used to formulate the element
- The method is used to model the load distribution in twenty-bolt joints
- The method was found to be robust, accurate and highly efficient

ACCEPTED MANUSCRIPT

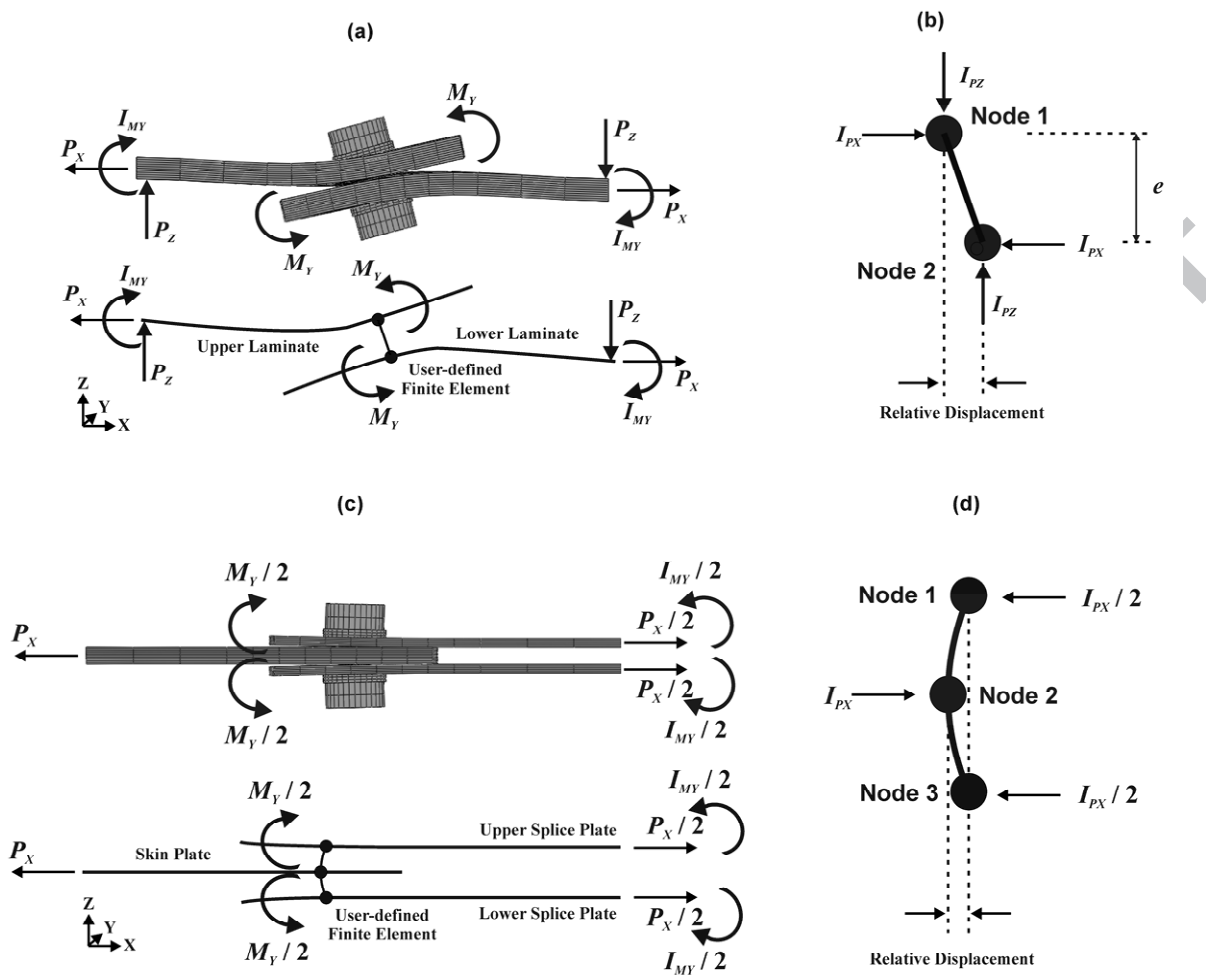




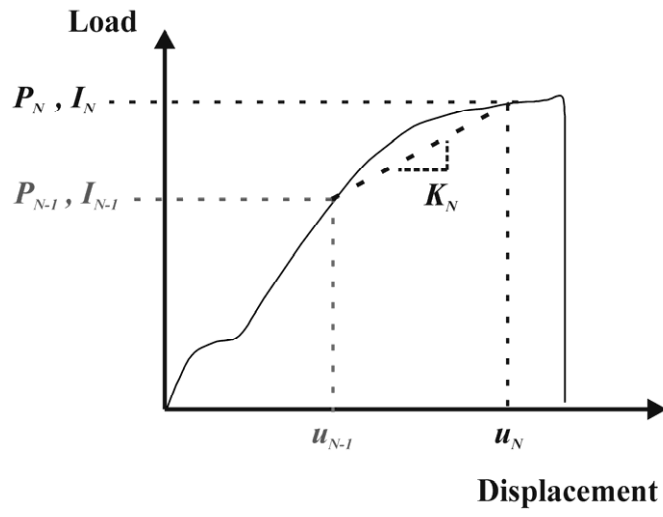
ACCEPTED MANUSCRIPT



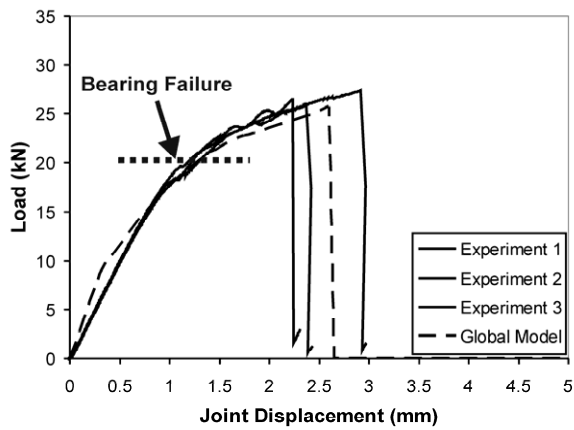
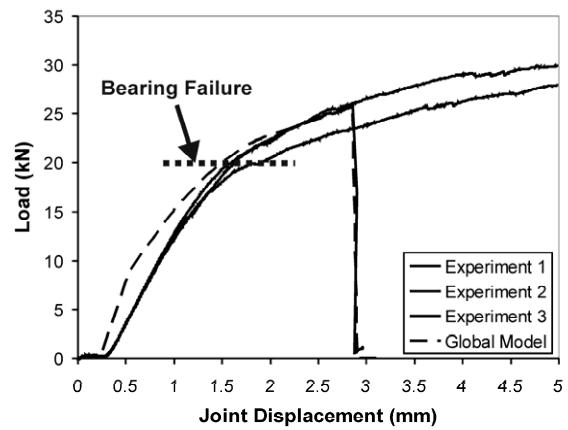
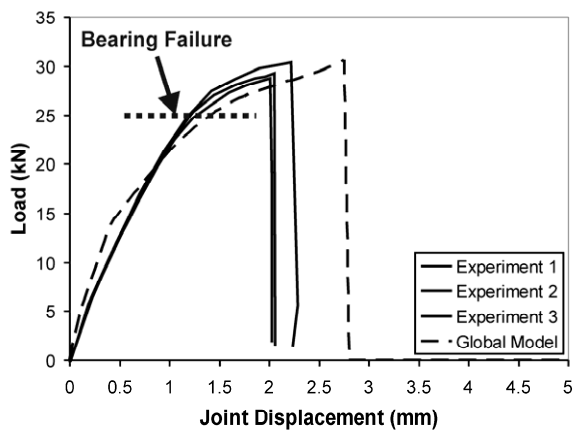
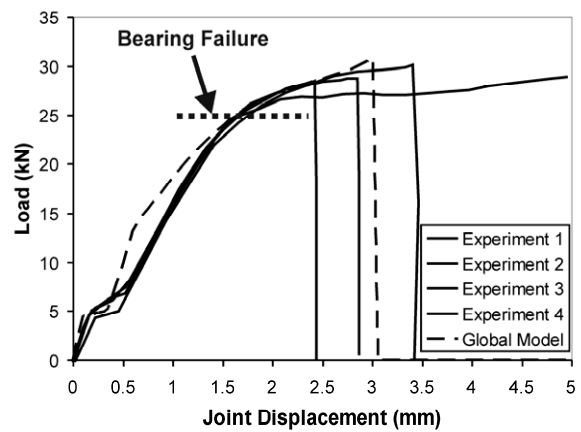
ACCEPTED MANUSCRIPT



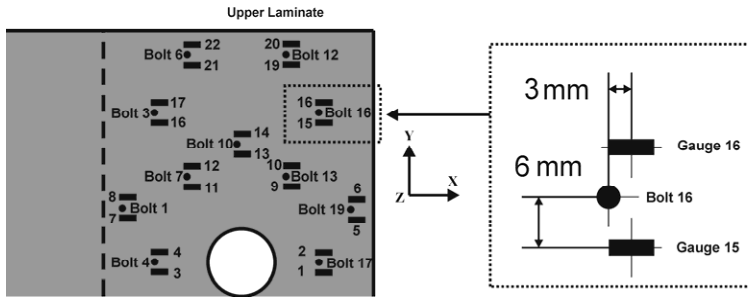
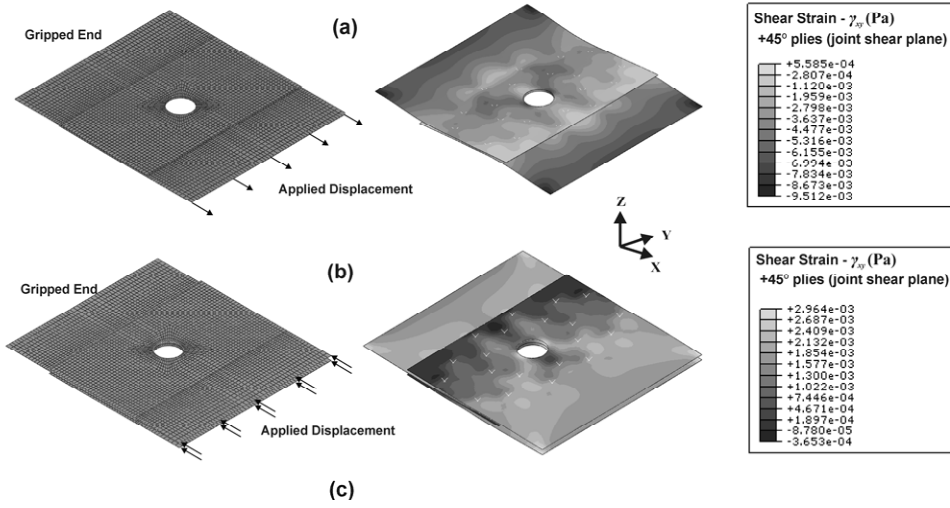
ACCEPTED

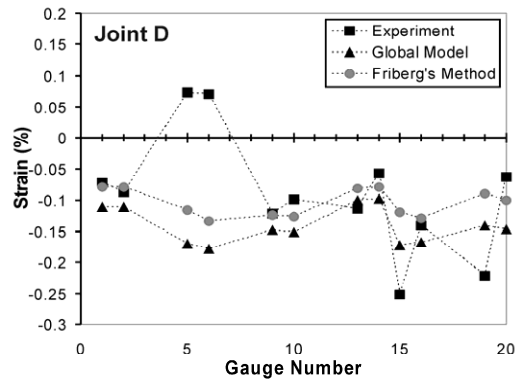
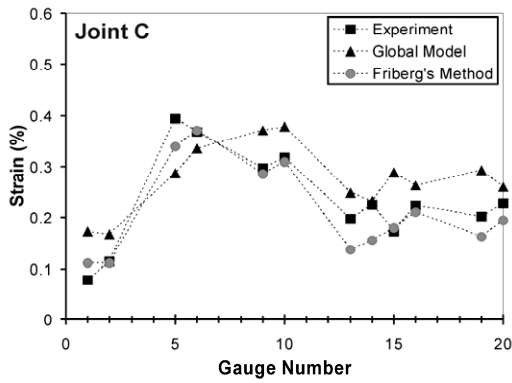
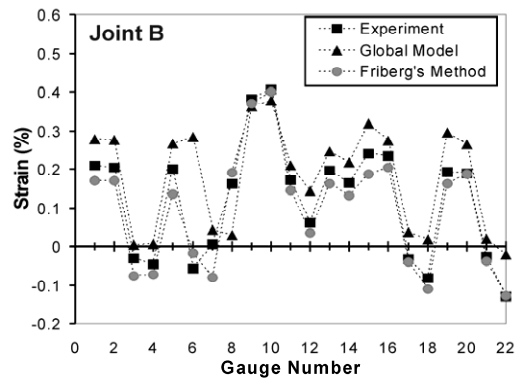
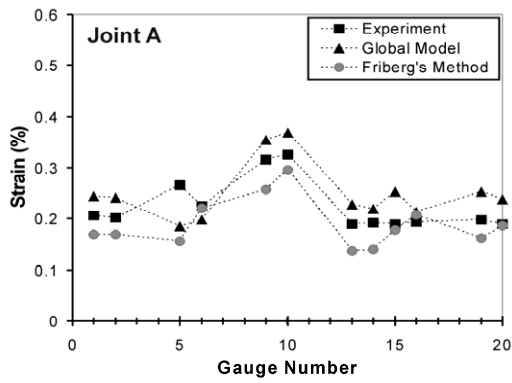


ACCEPTED MANUSCRIPT

(a) 10 $\mu\text{m}$  clearance, 7.2 MPa Pre-stress(b) 240 $\mu\text{m}$  clearance, 7.2 MPa Pre-stress(c) 10 $\mu\text{m}$  clearance, 227 MPa Pre-stress(d) 240 $\mu\text{m}$  clearance, 227 MPa Pre-stress

ACCEPTED





ACCEPTED MANUSCRIPT

